

Constitutive Modeling of Piezoelectric Polymer Composites

G.M. Odegard

*Michigan Technological University
Department of Mechanical Engineering – Engineering Mechanics
1400 Townsend Drive
Houghton, MI 49931*

Abstract

A new modeling approach is proposed for predicting the bulk electromechanical properties of piezoelectric composites. The proposed model offers the same level of convenience as the well-known Mori-Tanaka method. The electromechanical properties of four piezoelectric polymer composite materials are predicted with the proposed, Mori-Tanaka, Self-consistent methods, and detailed finite element analyses are conducted over full ranges of reinforcement volume fractions. The presented data offer a comprehensive comparison of the four modeling approaches for a wide range of matrix and reinforcement electromechanical properties, reinforcement geometry, and reinforcement volume fraction. By comparison with the finite element data, it is shown that the proposed model predicts properties that are, in some cases, more accurate than the Mori-Tanaka and Self-consistent schemes.

Keywords: Micromechanics; Mori-Tanaka; Piezoelectricity; PZT; PVDF; Self-consistent

Introduction

Piezoelectric materials are excellent candidates for use in sensors and actuators because of their ability to couple electrical and mechanical energy. For some applications, it is necessary to use composite materials in which one or more of the constituents have piezoelectric properties. To facilitate the design of these piezoelectric composite systems, convenient and accurate structure-property relationships must be developed.

Numerous attempts have been made to develop models to relate bulk electromechanical properties of composite materials to the electromechanical properties of individual constituents. Simple estimates, utilizing Voigt or Reuss-type approaches, have been used to predict the behavior of a limited class of composite geometries [1-4]. Upper and lower bounds for the electromechanical moduli have been determined [5-8]. Finite element analysis has also been used to predict electromechanical properties [9, 10]. Even though finite element analysis has the best potential for accurately predicting composite properties for any composite geometry, the solutions can be very expensive and time-consuming.

Several authors have extended Eshelby's [11] classical solution of an infinite medium containing a single ellipsoidal inclusion to include piezoelectric constituents [12-15]. Also referred to as the dilute solution, this approach ignores the interactions of the inclusions that occur at finite inclusion volume fractions. Other studies [14, 16-19] have focused on the classical extensions of Eshelby's solution for finite inclusion volume fractions, i.e., the Mori-Tanaka [20, 21], Self-

consistent [22, 23], and differential [24, 25] approaches. Analytical solutions for specific composite systems have also been determined [26-32]. Even though the overall framework of these approaches provides estimates for a wide range of inclusion sizes, geometries, and orientations, each of these methods suffers from drawbacks associated with accuracy and computational convenience.

In this paper, a model is proposed for predicting the coupled electromechanical properties of piezoelectric composites. This model is an extension of a technique originally developed for predicting mechanical properties of composites by generalizing the Mori-Tanaka and Self-consistent approaches [33]. First, the overall constitutive modeling of piezoelectric materials is discussed, followed by a description of the proposed model. Finally, the electromechanical properties of four different piezoelectric composite systems are predicted using the proposed, Mori-Tanaka, Self-consistent, and finite element models. The four piezoelectric composite systems used in this study were chosen to represent a wide range of practical materials: a graphite/Poly(vinylidene fluoride) (PVDF) composite, a Silicon Carbide (SiC)/PVDF particulate composite, a fibrous Lead Zirconate Titanate (PZT)/polyimide composite, and a PZT/polyimide particulate composite.

Constituent materials

The matrix and inclusion constituents used in this study were chosen such that the composite materials had four combinations of piezoelectric constituents and reinforcement geometries. The graphite/PVDF and SiC/PVDF composites have a piezoelectric polymer matrix with fiber and particle reinforcement, respectively. The PZT/polyimide composites have a piezoelectric inclusion with fiber and particle reinforcements.

PVDF is a orthotropic, semi-crystalline polymer which exhibits a piezoelectric effect with an electric field applied along the 3-axis. Typical electromechanical properties of PVDF are given in Table 1 (these properties were supplied by NASA Langley Research Center). LaRC-SI is a thermoplastic polyimide that was developed for aerospace applications. The properties of LaRC-SI used in this study correspond to the system with a 3% stoichiometric imbalance at room temperature [34] and are also shown in Table 1. The PVDF polymer was reinforced with both infinitely-long graphite fibers and spherical SiC particles. The fibers were unidirectionally aligned along the PVDF 1-axis. This alignment was chosen for the modeling because of the desire to maintain a high level of material compliance (therefore maximizing the piezoelectric effect) in the transverse directions, while providing reinforcement in the direction in which little piezoelectric effect and maximum mechanical reinforcement are required. The LaRC-SI polymer was reinforced with both infinitely-long PZT-7A fibers and spherical PZT-7A particles. PZT-7A is a ceramic that exhibits a piezoelectric effect with electric fields applied along all three principle axes. The PZT-7A fibers were unidirectionally aligned with the fiber 3-axis as the fiber-length axis. This alignment was chosen to maintain consistency with previous analyses [8, 14, 19], which ultimately provides alignment of the fibers during the poling process in the fabrication of these materials. All of the inclusion electromechanical properties are given in Table 1.

Micromechanics modeling

1. Piezoelectric materials

There are three standard notation systems that are commonly used to describe the constitutive modeling of linear-piezoelectric materials. Using the conventional indicial notation in which repeated subscripts are summed over the range of $i,j,m,n = 1,2,3$, the constitutive equations are

$$\begin{aligned}\sigma_{ij} &= C_{ijmn}\varepsilon_{mn} + e_{nij}E_n \\ D_i &= e_{imn}\varepsilon_{mn} - \kappa_{in}E_n\end{aligned}\quad (1)$$

where σ_{ij} , ε_{ij} , E_i , and D_i are the stress tensor, strain tensor, electric field vector, and the electric displacement vector, respectively. The quantities C_{ijmn} , e_{nij} , and κ_{in} are the elastic stiffness tensor, the piezoelectric tensor, and the permittivity tensor, respectively. The divergence equations, which are the elastic equilibrium and Gauss' law, are, respectively,

$$\begin{aligned}\sigma_{ij,j} &= 0 \\ D_{i,i} &= 0\end{aligned}\quad (2)$$

where the subscripted comma denotes partial differentiation. The gradient equations, which are the strain-displacement equations and electric field-potential, are, respectively,

$$\begin{aligned}\varepsilon_{ij} &= \frac{1}{2}(u_{i,j} + u_{j,i}) \\ E_i &= -\phi_{,i}\end{aligned}\quad (3)$$

where u_i and ϕ are the mechanical displacement and electric potential, respectively.

In the modeling of piezoelectric materials, it is more convenient to restate Eqn. (1) so that the elastic and electric variables are combined to yield a single constitutive equation. This notation is identical to the conventional indicial notation with the exception that lower case subscripts retain the range of 1-3 and capitalized subscripts take on the range of 1-4, with repeated capitalized subscripts summed over 1-4. In this notation, Eqn. (1) is

$$\Sigma_{iJ} = E_{iJMn}Z_{Mn}\quad (4)$$

where Σ_{iJ} , E_{iJMn} , and Z_{Mn} are, respectively,

$$\Sigma_{iJ} = \begin{cases} \sigma_{ij} & J = 1, 2, 3 \\ D_i & J = 4 \end{cases}\quad (5)$$

$$E_{iJMn} = \begin{cases} C_{ijmn} & J, M = 1, 2, 3 \\ e_{nij} & J = 1, 2, 3; M = 4 \\ e_{imn} & J = 4; M = 1, 2, 3 \\ -\kappa_{in} & J, M = 4 \end{cases} \quad (6)$$

$$Z_{Mn} = \begin{cases} \varepsilon_{mn} & M = 1, 2, 3 \\ E_n & M = 4 \end{cases} \quad (7)$$

The piezoelectric constitutive equation can be further simplified by expressing Eqn. (4) in matrix notation

$$\mathbf{\Sigma} = \mathbf{E}\mathbf{Z} \quad (8)$$

where the boldface indicates either a 9×9 matrix (\mathbf{E}) or a 9×1 column vector ($\mathbf{\Sigma}$, \mathbf{Z})

$$\mathbf{\Sigma}' = [\sigma_{11} \quad \sigma_{22} \quad \sigma_{33} \quad \sigma_{23} \quad \sigma_{13} \quad \sigma_{12} \mid D_1 \quad D_2 \quad D_3] \quad (9)$$

$$\mathbf{Z}' = [\varepsilon_{11} \quad \varepsilon_{22} \quad \varepsilon_{33} \quad \gamma_{23} \quad \gamma_{13} \quad \gamma_{12} \mid E_1 \quad E_2 \quad E_3] \quad (10)$$

$$\mathbf{E} = \left[\begin{array}{c|c} \mathbf{C} & \mathbf{e}^t \\ \hline \mathbf{e} & -\boldsymbol{\kappa} \end{array} \right] \quad (11)$$

$(6 \times 6) \quad (6 \times 3)$
 $(3 \times 6) \quad (3 \times 3)$

In Eqn. (11), \mathbf{C} , \mathbf{e} , and $\boldsymbol{\kappa}$ denote the elastic stiffness matrix, the piezoelectric constant matrix, and the permittivity matrix, respectively. The superscript t denotes a matrix transposition. Note that $\gamma_{ij} = 2\varepsilon_{ij}$ in order to keep \mathbf{E} a symmetric matrix. From Eqns (8) - (11), the constitutive equation for an orthotropic piezoelectric material is

$$\begin{bmatrix} \sigma_{11} \\ \sigma_{22} \\ \sigma_{33} \\ \sigma_{23} \\ \sigma_{13} \\ \sigma_{12} \\ D_1 \\ D_2 \\ D_3 \end{bmatrix} = \begin{bmatrix} C_{11} & C_{12} & C_{13} & 0 & 0 & 0 & 0 & 0 & e_{31} \\ C_{12} & C_{22} & C_{23} & 0 & 0 & 0 & 0 & 0 & e_{32} \\ C_{13} & C_{23} & C_{33} & 0 & 0 & 0 & 0 & 0 & e_{33} \\ 0 & 0 & 0 & C_{44} & 0 & 0 & 0 & e_{15} & 0 \\ 0 & 0 & 0 & 0 & C_{55} & 0 & e_{15} & 0 & 0 \\ 0 & 0 & 0 & 0 & 0 & C_{66} & 0 & 0 & 0 \\ \hline 0 & 0 & 0 & 0 & e_{15} & 0 & -\kappa_1 & 0 & 0 \\ 0 & 0 & 0 & e_{15} & 0 & 0 & 0 & -\kappa_2 & 0 \\ e_{31} & e_{32} & e_{33} & 0 & 0 & 0 & 0 & 0 & -\kappa_3 \end{bmatrix} \begin{bmatrix} \varepsilon_{11} \\ \varepsilon_{22} \\ \varepsilon_{33} \\ \gamma_{23} \\ \gamma_{13} \\ \gamma_{12} \\ E_1 \\ E_2 \\ E_3 \end{bmatrix} \quad (12)$$

where the contracted Voigt notation is used. In Eqn. (12), the 3-axis is aligned with the principle direction of polarization.

2. Electromechanical properties of composites

Using the direct approach [14, 35, 36] for the estimate of overall properties of heterogeneous materials, the volume-averaged piezoelectric fields of the composite with a total of N phases are

$$\bar{\Sigma} = \sum_{r=1}^N c_r \bar{\Sigma}_r \quad (13)$$

$$\bar{\mathbf{Z}} = \sum_{r=1}^N c_r \bar{\mathbf{Z}}_r \quad (14)$$

where c_r is the volume fraction of phase r , the overbar denotes a volume-averaged quantity, the subscript r denotes the phase, and $r = 1$ is the matrix phase. The constitutive equation for each phase is given by Eqn. (8). For a piezoelectric composite subjected to homogeneous elastic strain and electric field boundary conditions, \mathbf{Z}^0 , it has been shown that $\bar{\mathbf{Z}} = \mathbf{Z}^0$ [16]. The constitutive equation for the piezoelectric composite can be expressed in terms of the volume-averaged fields

$$\bar{\Sigma} = \mathbf{E} \bar{\mathbf{Z}} \quad (15)$$

The volume-average strain and electric field in phase r is

$$\bar{\mathbf{Z}}_r = \mathbf{A}_r \bar{\mathbf{Z}} \quad (16)$$

where \mathbf{A}_r is the concentration tensor of phase r , and

$$\sum_{r=1}^N c_r \mathbf{A}_r = \mathbf{I} \quad (17)$$

where \mathbf{I} is the identity tensor. Combining Eqns. (13)-(17) yields the electromechanical modulus of the composite in terms of the constituent moduli

$$\mathbf{E} = \mathbf{E}_1 + \sum_{r=2}^N c_r (\mathbf{E}_r - \mathbf{E}_1) \mathbf{A}_r \quad (18)$$

Various procedures exist for evaluating the concentration tensor. The most widely used approaches are the Mori-Tanaka and Self-consistent schemes.

For the Mori-Tanaka approach, the concentration tensor is

$$\mathbf{A}_s = \mathbf{A}_r^{dil} \left[c_1 \mathbf{I} + \sum_{r=2}^N c_r \mathbf{A}_r^{dil} \right]^{-1} \quad (19)$$

where \mathbf{A}_r^{dil} is the dilute concentration tensor given by

$$\mathbf{A}_r^{dil} = \left[\mathbf{I} + \mathbf{S}_r \mathbf{E}_1^{-1} (\mathbf{E}_r - \mathbf{E}_1) \right]^{-1} \quad (20)$$

In Eqn. (20) \mathbf{S}_r is the constraint tensor for phase r , which is analogous to the Eshelby tensor used in determining elastic properties of composite materials [11]. The constraint tensor is evaluated as a function of the lengths of the principle axes of the reinforcing phase r , a_i^r , and the electromechanical properties of the surrounding matrix

$$\mathbf{S}_r = f(\mathbf{E}_1, a_1^r, a_2^r, a_3^r) \quad (21)$$

The complete expression for Eqn. (21) is given elsewhere [16]. While the Mori-Tanaka approach provides for a quick and simple calculation of the bulk composite electromechanical properties, it has been shown that it yields predicted mechanical properties that are relatively low and high for composites with stiffer inclusions and matrix, respectively [33]. This issue could possibly lead to less accurate estimations of the electromechanical moduli, especially for relatively large inclusion volume fractions [37-39].

In the Self-consistent scheme, the concentration tensor is

$$\mathbf{A}_r = \left[\mathbf{I} + \mathbf{S}_r \mathbf{E}^{-1} (\mathbf{E}_r - \mathbf{E}) \right]^{-1} \quad (22)$$

where \mathbf{E} is the unknown electromechanical moduli of the composite, and the constraint tensor, \mathbf{S}_r , is evaluated as a function of \mathbf{E} and a_i^r . Since the electromechanical moduli of the composite appears in both Eqns. (22) and (18), iterative schemes or numerical techniques are ultimately required for the prediction of the electromechanical moduli of composites using the Self-consistent method. This approach results in slow and complicated calculations.

It has been demonstrated [33] that a more general form of the concentration tensor can be used for the prediction of mechanical properties of composites. Extending this concept to the prediction of electromechanical properties results in

$$\mathbf{A}_r = \left[\mathbf{I} + \mathbf{S}_r \mathbf{E}_0^{-1} (\mathbf{E}_r - \mathbf{E}_0) \right]^{-1} \quad (23)$$

where \mathbf{E}_0 is the electroelastic moduli of the reference medium, and the constraint tensor is evaluated using \mathbf{E}_0 and a_i^r . Therefore, it is assumed that the reference medium is the material

that immediately surrounds the inclusion for the evaluation of the constraint and concentration tensors. Naturally, the electroelastic moduli of the reference medium can have a wide range of values, however, it is most realistic to assume that they are similar to the moduli of the overall composite, as is the case in the Self-consistent method.

For convenience, a simple, yet accurate, estimation of the overall electroelastic moduli can be chosen for the reference medium so that the overall properties of the piezoelectric composite can be calculated using Eqns. (18) and (23). Even though a simple and accurate estimation of the reference medium means that the electroelastic moduli can be calculated without Eqns. (18) and (23), this framework allows for the computation of the moduli for various inclusion sizes, geometries, and orientations. The reference medium is approximated with a set of equations that are similar to the Halpin-Tsai relation [40], which is extended here for multiple inclusions and piezoelectric composites

$$E_{ijkl}^0 = E_{ijkl}^1 \frac{1 + \sum_{r=2}^N \eta_{ijkl}^r c_r}{1 - \sum_{r=2}^N \eta_{ijkl}^r c_r} \quad (24)$$

where

$$\eta_{ijkl}^r = \frac{E_{ijkl}^r - E_{ijkl}^1}{E_{ijkl}^r + E_{ijkl}^1} \quad (25)$$

Eqns. (24) and (25) indicate that as $c_1 \rightarrow 1$ and $c_r \rightarrow 1$, $E_{ijkl}^0 \rightarrow E_{ijkl}^1$ and $E_{ijkl}^0 \rightarrow E_{ijkl}^r$, respectively.

Eqns. (18) and (23)-(25) were used to calculate the electromechanical properties for the four composite systems for inclusion volume fractions ranging from 0% to the maximum theoretical limits, which are about 90% and 75% for fibrous and particulate composites, respectively. The constraint tensor in Eqn. (23) was evaluated numerically using Gaussian quadrature [41]. The fibers were modeled as infinitely long cylinders and the particles were modeled as spheres. Perfect bonding between the inclusions and matrix was assumed.

Finite element analysis

Another approach to estimate the electromechanical properties of piezoelectric composites is finite element analysis of a representative volume element (RVE) of the material. Whereas the methods of the previous section provide relatively quick predictions by assuming that the stress and strain fields inside the inclusions are constant, finite element analysis predicts these fields in the inclusion and matrix, and thus, provides a more realistic prediction to the overall electromechanical moduli of the composite. This added accuracy comes at a price, however, since each independent property of the piezoelectric composite (16 independent parameters are shown in Eqn. (12)) must be determined by a single finite element analysis. In parametric studies where many combinations of inclusion shape and volume fraction must be considered,

the finite element approach can become very time-consuming and expensive. Therefore, in this study, the finite element results are used to check the accuracy of the modeling methods discussed in the previous section.

The finite element model was developed and executed using ANSYS[®] 7.0. Representative volume elements (RVEs) of fiber- and particulate-reinforced composites were meshed using 10-noded electromechanical tetrahedral elements with 40 degrees of freedom, three displacements and an electric potential at each node (SOLID98). The fibrous composite RVE (Fig. 1) simulated a hexagonal packing arrangement, with a maximum fiber volume fraction of about 90%. The particulate composite RVE (Fig. 2) had hexagonal packing in one plane with a maximum particle volume fraction of about 60%. For each finite element analysis, the desired volume fraction was obtained by adjusting the dimensions of the RVE while keeping the reinforcement size constant. The properties of the materials are shown in Table 1. Additional reinforcement and matrix material were connected to each of the eight faces of both the fibrous and particulate RVEs to form the full finite element models (Figs. 1 and 2).

For homogeneous applied elastic strains and electric fields, the displacements and voltages on the boundary of the full finite element models were, respectively,

$$\begin{aligned} u_i(B) &= \varepsilon_{ij}^{\circ} x_j \\ \phi(B) &= -E_i^{\circ} x_i \end{aligned} \quad (26)$$

where B indicates the boundary of the full finite element model. A total of 16 boundary conditions were applied to the finite element models for each combination of material type and volume fraction. Each boundary condition was used to predict one of the independent electroelastic constants in Eqn. (12). The electroelastic constants and the corresponding applied strains, electric fields, and the boundary conditions calculated using Eqn. (26) are listed in Tables 2 to 6. For each set of boundary conditions, all unspecified strains and electric fields in Tables 2 to 6 are zero. It is noted at this point that the boundary conditions specified in Eqn. (26) are often referred to as *kinematic* boundary conditions. These boundary conditions are not applied directly to the boundary of the RVE. Instead, they are applied to the boundary of the full finite element model. Therefore, the resulting deformations of the RVE are not over-constrained. Over-constrained RVE edges are a result of applying the kinematic boundary conditions directly to the boundary of the RVE [42].

The elastic strain energy, dielectric energy, and electromechanical energy of a piezoelectric material are, respectively,

$$\begin{aligned} U_e &= \sum_{m=1}^n U_e^m = \frac{V}{2} C_{ijkl} \varepsilon_{ij}^{\circ} \varepsilon_{kl}^{\circ} \\ U_d &= \sum_{m=1}^n U_d^m = \frac{V}{2} \kappa_{ij} E_i^{\circ} E_j^{\circ} \\ U_{em} &= \sum_{m=1}^n U_{em}^m = \frac{V}{2} e_{ijk} \varepsilon_{jk}^{\circ} E_i^{\circ} \end{aligned} \quad (27)$$

where U^m is the energy of element m , n is the total number of finite elements in the RVE, and V is the volume of the RVE. The energies were calculated for each element in the RVE volumes for each set of boundary conditions (Tables 2 to 6) applied to the full finite element model boundary. The total energies of the RVEs were determined by summing the energies of each RVE element, as indicated by the first equality in Eqn. (27). The corresponding elastic, dielectric, and piezoelectric constants were subsequently calculated using the second equality in Eqn. (27).

Results and Discussion

The Young's moduli, Y_1 , Y_2 , and Y_3 ; shear moduli, G_{23} , G_{13} , and G_{12} ; piezoelectric constants, e_{15} , e_{31} , e_{32} , e_{33} ; and dielectric constants, κ_1/κ_0 , κ_2/κ_0 , and κ_3/κ_0 ; for the four materials discussed in this paper are presented below. The subscripts of these quantities indicate the corresponding axes, as shown in Eqn. (12), and the permittivity of free space, κ_0 , is $8.85 \times 10^{-12} \text{ C/m}^2$.

1. Graphite/PVDF fiber composite

The Young's moduli of the graphite/PVDF composite are shown in Fig. 3 as a function of the graphite fiber volume fraction for the results obtained with the finite element analysis, the proposed model discussed above, the Mori-Tanaka model, and the Self-consistent method. For the Young's modulus parallel to the fiber-alignment direction, Y_1 , all four models predict the same values for the entire range of fiber volume fractions. For the two transverse moduli, Y_2 and Y_3 , the Mori-Tanaka and finite element models match very well for the entire range of fiber volume fractions, while the proposed and Self-consistent models over-predict the Young's moduli for fiber volume fractions over 40%.

The shear moduli of this material for the entire range of fiber volume fractions are shown in Fig. 4. For the longitudinal shear moduli, G_{13} and G_{12} , the proposed model has a closer agreement with the finite element model than the Mori-Tanaka and Self-consistent models have with the finite element model for fiber volume fractions above 40%. For the transverse shear modulus, G_{23} , the proposed, Mori-Tanaka, and the Self-consistent all predict slight higher values than the finite element model, with the Mori-Tanaka showing the closest agreement.

The piezoelectric constants, e_{31} , e_{32} , and e_{33} , are shown in Fig. 5 as a function of the fiber volume fraction. The four models predict nearly equal values of e_{31} and e_{32} over the entire range. For the piezoelectric constant e_{33} , the proposed and Self-consistent results over-predict the finite element model, while the Mori-Tanaka method shows good agreement with the finite element model.

The dielectric constants, κ_1/κ_0 , κ_2/κ_0 , and κ_3/κ_0 , are shown in Fig. 6. All four models predict identical values for all three dielectric constants for the complete range of fiber volume fractions.

2. SiC/PVDF particle composite

The Young's moduli of the SiC/PVDF composite are shown in Fig.7 as a function of particle volume fraction. At particle volume fractions of about 20% and lower, all four models predict nearly identical moduli. At higher particle volume fractions, the proposed model predicts moduli that have closer agreement with the finite element results than has the predicted values from the Mori-Tanaka model. For particle volume fractions higher than 20%, the Self-consistent approach significantly over-predicts the other three models.

The three shear moduli are shown in Fig. 8 for the entire range of particle volume fractions. For all three shear moduli, at volume fractions of 50% and less, the Mori-Tanaka and finite element models have close agreement, with the proposed model over-predicting the shear moduli. For a volume fraction of 60%, the shear moduli of the finite element model start increasing dramatically, and the proposed model shows closer agreement with the finite element model than does the Mori-Tanaka approach. For particle volume fractions over 20%, the Self-consistent approach significantly over-estimates all three shear moduli.

The piezoelectric constants are shown in Fig. 9 as a function of particle volume fraction. For the constant e_{31} , the proposed model data matches the finite element data more closely than does the Mori-Tanaka and Self-consistent approaches. For the constant e_{32} , all four models predict nearly identical values for the entire range of particle volume fractions. For the piezoelectric constant e_{33} , the Mori-Tanaka approach exhibits the closest agreement with the finite element predictions, especially for particle volume fractions above 30%.

The three dielectric constants for the composite are shown in Fig. 10. Similar to the graphite/PVDF composite, all four models predict identical values for all three dielectric constants for the entire range of particle volume fractions.

3. PZT-7A/polyimide fiber composite

The Young's moduli of the PZT-7A composite are shown in Fig. 11 for the entire range of fiber volume fractions. For the longitudinal Young's modulus, Y_3 , all three models predict the same values over the complete range of volume fractions. For the transverse Young's moduli, Y_1 and Y_2 , the Mori-Tanaka and finite element models have close agreement up to a fiber volume fraction of 80%. At a fiber volume fraction of 90%, the proposed model exhibits the closest agreement to the finite element model. The Self-consistent method significantly over-predicts the finite element model at fiber volume fractions above 50%.

The shear moduli of the composite are plotted as a function of fiber volume fraction in Fig. 12. For the longitudinal shear moduli, G_{23} and G_{13} , and the transverse shear modulus, G_{12} , the proposed, Mori-Tanaka, and Self-consistent models over-predict the finite element model for the entire range of volume fractions. While the Mori-Tanaka model exhibits the closest agreement with the finite element model, the Self-consistent significantly over-estimates the finite element model data.

The piezoelectric constants of this material are shown in Fig. 13. For the constants $e_{31} = e_{32}$ and e_{33} , all four models predict very similar values for the entire range of fiber volume fractions. For e_{15} , both the proposed and Mori-Tanaka models closely agree with the finite element model for the entire range of volume fractions. The Self-consistent method significantly over-estimates e_{15} for the fiber volume fractions above 30%.

The dielectric constants are shown in Fig. 14 as a function of fiber volume fraction. For the transverse dielectric constants, κ_1/κ_0 and κ_2/κ_0 , the Mori-Tanaka model predicts the finite element model data better than does the proposed and Self-consistent models for fiber volume fractions above 50%. For the longitudinal dielectric constant, κ_3/κ_0 , the four models predict nearly identical values over the entire range of volume fractions.

4. PZT-7A/polyimide particle composite

The Young's moduli of the PZT-7A/LaRC-SI particulate composite are shown in Fig. 15 as a function of particle volume fraction. For both the transverse Young's moduli, Y_1 and Y_2 , and the longitudinal Young's modulus, Y_3 , the proposed model agrees closely with the finite element model for the entire range of particle volume fractions considered. The Mori-Tanaka and Self-consistent models significantly under-predict and over-predict, respectively, the finite element data for volume fractions above 50%.

The shear moduli of this material for the range of volume fractions are shown in Fig. 16. For the longitudinal shear moduli, G_{23} and G_{13} , and the transverse shear modulus, G_{12} , the proposed, Mori-Tanaka, and Self-consistent models over-predict the finite element model data for the entire range of considered particle volume fractions, with the Mori-Tanaka exhibiting the closest agreement. For particle volume fractions above 20%, the Self-consistent model significantly over-predicts both the longitudinal and transverse shear moduli.

The piezoelectric constants are shown in Fig. 17 as a function of particle volume fraction. For all four constants, e_{15} , $e_{31} = e_{32}$, and e_{33} , the finite element, proposed, and Mori-Tanaka models show close agreement up to a particle volume fraction of 40%. For the constants e_{15} and e_{32} , the Mori-Tanaka model has the closest agreement with the finite element model in the particle volume fraction range between 40% and 50%. At a particle volume fraction of 60%, the proposed model exhibits the closest agreement with the finite element model. For $e_{31} = e_{32}$, the proposed model shows the closest match with the finite element model for particle volume fractions above 40%. For particle volume fractions above 20%, the Self-consistent results are dramatic and do not appear to closely predict any of the piezoelectric constants.

The dielectric constants of the material are shown in Fig. 18. For the transverse dielectric constants, κ_1/κ_0 and κ_2/κ_0 , and the longitudinal dielectric constant, κ_3/κ_0 , the predicted values from the Mori-Tanaka model agree with the finite element model up to a particle volume fraction of about 50%. Above that value, the Mori-Tanaka model under-predicts the finite element data for κ_1/κ_0 and κ_2/κ_0 . At that point, the proposed model exhibits better agreement with the finite element model. For particle volume fractions above 20%, the Self-consistent approach significantly over-estimates both transverse and longitudinal dielectric constants.

Summary and Conclusions

A new modeling approach has been proposed for predicting the bulk electromechanical properties of piezoelectric composites. The proposed model offers the same level of convenience as the Mori-Tanaka method, that is, it does not require iterative or numerical schemes for obtaining the predicted properties, as is required with the Self-consistent and differential schemes. The electromechanical properties of four piezoelectric polymer composite materials were predicted with the proposed, Mori-Tanaka, Self-consistent methods, and detailed finite element analyses for a wide range of matrix and reinforcement electromechanical properties, geometry, and volume fraction. The four piezoelectric composite materials considered were: a graphite/PVDF composite, a SiC/PVDF particulate composite, a fibrous PZT-7A/LaRC-SI composite, and a PZT-7A/LaRC-SI particulate composite.

It was shown that the proposed model yields predicted properties that were, in some cases, more accurate than the Mori-Tanaka and Self-consistent schemes. In particular, the proposed model exhibits equal or closer agreement with the finite element model than does the Mori-Tanaka and Self-consistent schemes for the prediction of several electromechanical properties. For the PVDF matrix composites these properties include the longitudinal shear and longitudinal Young's moduli and all dielectric constants for the graphite/PVDF composite; and all Young's moduli, all shear moduli (for volume fractions above 50%), the piezoelectric constants e_{31} and e_{32} , and all dielectric constants for the SiC/PVDF composite. For the PZT-reinforced composites these include the longitudinal Young's modulus, the piezoelectric constants e_{33} and e_{15} , and the longitudinal dielectric constant of the fibrous PZT-7A/LaRC-SI composite; and all of the Young's moduli, all of the piezoelectric constants, and the longitudinal dielectric constant (for volume fractions above 60%) of the particulate PZT-7A/LaRC-SI composite. Based on these results, the choice of the most accurate model (between the proposed, Mori-Tanaka, and Self-consistent methods) for a specific piezoelectric composite material should be based on the constituent properties and the geometry and volume fraction of the inclusions.

References

- [1] Newnham, R.E.; Skinner, D.P., and Cross, L.E.: Connectivity and Piezoelectric-Pyroelectric Composites. *Materials Research Bulletin*. Vol. 13, 1978, pp. 525-536.
- [2] Banno, H.: Recent Developments of Piezoelectric Ceramic Products and Composites of Synthetic Rubber and Piezoelectric Ceramic Particles. *Ferroelectrics*. Vol. 50, 1983, pp. 329-338.
- [3] Chan, H.L.W. and Unsworth, J.: Simple Model for Piezoelectric Ceramic/Polymer 1-3 Composites Used in Ultrasonic Transducer Applications. *IEEE Transactions on Ultrasonics, Ferroelectrics, and Frequency Control*. Vol. 36, 1989, pp. 434-441.
- [4] Smith, W.A. and Auld, B.A.: Modeling 1-3 Composite Piezoelectrics: Thickness-Mode Oscillations. *IEEE Transactions on Ultrasonics, Ferroelectrics, and Frequency Control*. Vol. 38, 1991, pp. 40-47.
- [5] Olson, T. and Avellaneda, M.: Effective Dielectric and Elastic Constants of Piezoelectric Polycrystals. *Journal of Applied Physics*. Vol. 71, 1992, pp. 4455-4464.
- [6] Bisegna, P. and Luciano, R.: Variational Bounds for the Overall Properties of Piezoelectric Composites. *Journal of the Mechanics and Physics of Solids*. Vol. 44, 1996, pp. 583-602.
- [7] Hori, M. and Nemat-Nasser, S.: Universal Bounds for Effective Piezoelectric Moduli. *Mechanics of Materials*. Vol. 30, 1998, pp. 1-19.
- [8] Li, J.Y. and Dunn, M.L.: Variational Bounds for the Effective Moduli of Heterogeneous Piezoelectric Solids. *Philosophical Magazine, A: Physics of Condensed Matter, Structure, Defects, and Mechanical Properties*. Vol. 81, 2001, pp. 903-926.
- [9] Gaudenzi, P.: On the Electromechanical Response of Active Composite Materials with Piezoelectric Inclusions. *Computers and Structures*. Vol. 65, 1997, pp. 157-168.
- [10] Poizat, C. and Sester, M.: Effective Properties of Composites with Embedded Piezoelectric Fibres. *Computational Materials Science*. Vol. 16, 1999, pp. 89-97.
- [11] Eshelby, J.D.: The Determination of the Elastic Field of an Ellipsoidal Inclusion, and Related Problems. *Proceedings of the Royal Society of London, Series A*. Vol. 241, 1957, pp. 376-396.
- [12] Wang, B.: Three-Dimensional Analysis of an Ellipsoidal Inclusion in a Piezoelectric Material. *International Journal of Solids and Structures*. Vol. 29, 1992, pp. 293-308.
- [13] Benveniste, Y.: The Determination of the Elastic and Electric Fields in a Piezoelectric Inhomogeneity. *Journal of Applied Physics*. Vol. 72, 1992, pp. 1086-1095.
- [14] Dunn, M.L. and Taya, M.: Micromechanics Predictions of the Effective Electroelastic Moduli of Piezoelectric Composites. *International Journal of Solids and Structures*. Vol. 30, No. 2, 1993, pp. 161-175.
- [15] Chen, T.: An Invariant Treatment of Interfacial Discontinuities in Piezoelectric Media. *International Journal of Engineering Science*. Vol. 31, 1993, pp. 1061-1072.
- [16] Dunn, M.L. and Taya, M.: An Analysis of Piezoelectric Composite Materials Containing Ellipsoidal Inhomogeneities. *Proceedings of the Royal Society of London, Series A*. Vol. 443, 1993, pp. 265-287.
- [17] Chen, T.: Micromechanical Estimates of the Overall Thermoelastoelectric Moduli of Multiphase Fibrous Composites. *International Journal of Solids and Structures*. Vol. 31, 1994, pp. 3099-3111.

- [18] Huang, J.H. and Kuo, W.S.: Micromechanics Determination of the Effective Properties of Piezoelectric Composites Containing Spatially Oriented Short Fibers. *Acta Materialia*. Vol. 44, 1996, pp. 4889-4898.
- [19] Fakri, N.; Azrar, L., and El Bakkali, L.: Electroelastic Behavior Modeling of Piezoelectric Composite Materials Containing Spatially Oriented Reinforcements. *International Journal of Solids and Structures*. Vol. 40, 2003, pp. 361-384.
- [20] Mori, T. and Tanaka, K.: Average Stress in Matrix and Average Elastic Energy of Materials with Misfitting Inclusions. *Acta Metallurgica*. Vol. 21, 1973, pp. 571-574.
- [21] Benveniste, Y.: A New Approach to the Application of Mori-Tanaka's Theory in Composite Materials. *Mechanics of Materials*. Vol. 6, 1987, pp. 147-157.
- [22] Hill, R.: A Self-Consistent Mechanics of Composite Materials. *Journal of the Mechanics and Physics of Solids*. Vol. 13, 1965, pp. 213-222.
- [23] Budiansky, B.: On the Elastic Moduli of Some Heterogeneous Materials. *Journal of the Mechanics and Physics of Solids*. Vol. 13, 1965, pp. 223-227.
- [24] McLaughlin, R.: A Study of the Differential Scheme for Composite Materials. *International Journal of Engineering Science*. Vol. 15, 1977, pp. 237-244.
- [25] Norris, A.N.: A Differential Scheme for the Effective Moduli of Composites. *Mechanics of Materials*. Vol. 4, 1985, pp. 1-16.
- [26] Dunn, M.L.: Electroelastic Green's Functions for Transversely Isotropic Piezoelectric media and Their Application to the Solution of Inclusion and Inhomogeneity Problems. *International Journal of Engineering Science*. Vol. 32, No. 1, 1994, pp. 119-131.
- [27] Wang, B.: Effective Behavior of Piezoelectric Composites. *Applied Mechanics Reviews*. Vol. 47, 1994, pp. S112-S121.
- [28] Dunn, M.L. and Wienecke, H.A.: Green's Functions for Transversely Isotropic Piezoelectric Solids. *International Journal of Solids and Structures*. Vol. 33, 1996, pp. 4571-4581.
- [29] Chen, T.: Effective Properties of Platelet Reinforced Piezocomposites. *Composites: Part B*. Vol. 27, 1996, pp. 467-474.
- [30] Dunn, M.L. and Wienecke, H.A.: Inclusions and Inhomogeneities in Transversely Isotropic Piezoelectric Solids. *International Journal of Solids and Structures*. Vol. 34, No. 27, 1997, pp. 3571-3582.
- [31] Mikata, Y.: Determination of Piezoelectric Eshelby Tensor in Transversely Isotropic Piezoelectric Solids. *International Journal of Engineering Science*. Vol. 38, 2000, pp. 605-641.
- [32] Mikata, Y.: Explicit Determination of Piezoelectric Eshelby Tensors for a Spheroidal Inclusion. *International Journal of Solids and Structures*. Vol. 38, 2001, pp. 7045-7063.
- [33] Dvorak, G.J. and Srinivas, M.V.: New Estimates of Overall Properties of Heterogeneous Solids. *Journal of the Mechanics and Physics of Solids*. Vol. 47, 1999, pp. 899-920.
- [34] Nicholson, L.M.; Whitley, K.S.; Gates, T.S., and Hinkley, J.A.: Influence of Molecular Weight on the Mechanical Performance of a Thermoplastic Glassy Polyimide. *Journal of Materials Science*. Vol. 35, No. 24, 2000, pp. 6111-6122.
- [35] Hill, R.: Elastic Properties of Reinforced Solids: Some Theoretical Principles. *Journal of the Mechanics and Physics of Solids*. Vol. 11, 1963, pp. 357-372.
- [36] Dvorak, G.J. and Benveniste, Y.: On Transformation Strains and Uniform Fields in Multiphase Elastic Media. *Proceedings of the Royal Society of London, Series A*. Vol. 437, 1992, pp. 291-310.

- [37] Christensen, R.M.: A Critical Evaluation for a Class of Micromechanics Models. *Journal of the Mechanics and Physics of Solids*. Vol. 38, 1990, pp. 379-404.
- [38] Christensen, R.M.; Schantz, H., and Shapiro, J.: On the Range of Validity of the Mori-Tanaka Method. *Journal of the Mechanics and Physics of Solids*. Vol. 40, 1992, pp. 69-73.
- [39] Benedikt, B.; Rupnowski, P., and Kumosa, M.: Visco-elastic Stress Distributions and Elastic Properties in Unidirectional Composites with Large Volume Fractions of Fibers. *Acta Materialia*. Vol. 51, No. 12, 2003, pp. 3483-3493.
- [40] Halpin, J.C. and Tsai, S.W.: Environmental Factors in Composites Design. AFML-TR-67-423, 1967.
- [41] Davis, P.J. and Polonsky, I.: Numerical Interpolation, Differentiation and Integration. In: *Handbook of Mathematical Functions with Formulas, Graphs, and Mathematical Tables*. M. Abramowitz and I. A. Stegun, eds. New York: John Wiley & Sons, 1972, pp. 875-924.
- [42] Sun, C.T. and Vaidya, R.S.: Prediction of Composite Properties from a Representative Volume Element. *Composites Science and Technology*. Vol. 56, 1996, pp. 171-179.

Table 1. Electromechanical properties of matrix and inclusion materials

Property	PVDF	LaRC-SI	Graphite fiber	SiC particle	PZT-7A
C_{11} (GPa)	3.8	8.1	243.7	483.7	148.0
C_{12} (GPa)	1.9	5.4	6.7	99.1	76.2
C_{13} (GPa)	1.0	5.4	6.7	99.1	74.2
C_{22} (GPa)	3.2	8.1	24.0	483.7	148.0
C_{23} (GPa)	0.9	5.4	9.7	99.1	74.2
C_{33} (GPa)	1.2	8.1	24.0	483.7	131.0
C_{44} (GPa)	0.7	1.4	11.0	192.3	25.4
C_{55} (GPa)	0.9	1.4	27.0	192.3	25.4
C_{66} (GPa)	0.9	1.4	27.0	192.3	35.9
κ_1/κ_0	7.4	2.8	12.0	10.0	460.0
κ_2/κ_0	9.3	2.8	12.0	10.0	460.0
κ_3/κ_0	7.6	2.8	12.0	10.0	235.0
e_{15} (C/m ²)	0.0	0.0	0.0	0.0	9.2
e_{31} (C/m ²)	0.024	0.0	0.0	0.0	-2.1
e_{32} (C/m ²)	0.001	0.0	0.0	0.0	-2.1
e_{33} (C/m ²)	-0.027	0.0	0.0	0.0	9.5

Table 2. Boundary conditions for axial stiffness components

Property	Applied strain and electric field	Displacements and electric potential	Elastic energy
C_{11}	$\varepsilon_{11}^o = \varepsilon^o$	$u_1(B) = \varepsilon^o x_1$ $u_2(B) = 0$ $u_3(B) = 0$ $\phi(B) = 0$	$U_e = \frac{V}{2} C_{11} (\varepsilon^o)^2$
C_{22}	$\varepsilon_{22}^o = \varepsilon^o$	$u_1(B) = 0$ $u_2(B) = \varepsilon^o x_2$ $u_3(B) = 0$ $\phi(B) = 0$	$U_e = \frac{V}{2} C_{22} (\varepsilon^o)^2$
C_{33}	$\varepsilon_{33}^o = \varepsilon^o$	$u_1(B) = 0$ $u_2(B) = 0$ $u_3(B) = \varepsilon^o x_3$ $\phi(B) = 0$	$U_e = \frac{V}{2} C_{33} (\varepsilon^o)^2$

Table 3. Boundary conditions for plane-strain bulk moduli

Property	Applied strain and electric field	Displacements and electric potential	Elastic energy
K_{23}	$\varepsilon_{22}^o = \varepsilon_{33}^o = \varepsilon^o$	$u_1(B) = 0$ $u_2(B) = \varepsilon^o x_2$ $u_3(B) = \varepsilon^o x_3$ $\phi(B) = 0$	$U_e = \frac{V}{2} K_{23} (\varepsilon^o)^2$
K_{13}	$\varepsilon_{11}^o = \varepsilon_{33}^o = \varepsilon^o$	$u_1(B) = \varepsilon^o x_1$ $u_2(B) = 0$ $u_3(B) = \varepsilon^o x_3$ $\phi(B) = 0$	$U_e = \frac{V}{2} K_{13} (\varepsilon^o)^2$
K_{12}	$\varepsilon_{11}^o = \varepsilon_{22}^o = \varepsilon^o$	$u_1(B) = \varepsilon^o x_1$ $u_2(B) = \varepsilon^o x_2$ $u_3(B) = 0$ $\phi(B) = 0$	$U_e = \frac{V}{2} K_{12} (\varepsilon^o)^2$

Table 4. Boundary conditions for shear stiffness components

Property	Applied strain and electric field	Displacements and electric potential	Elastic energy
C_{44}	$\varepsilon_{23}^{\circ} = \frac{\gamma^{\circ}}{2}$	$u_1(B) = 0$ $u_2(B) = (\gamma^{\circ}/2)x_3$ $u_3(B) = (\gamma^{\circ}/2)x_2$ $\phi(B) = 0$	$U_e = \frac{V}{2} C_{44} (\gamma^{\circ})^2$
C_{55}	$\varepsilon_{13}^{\circ} = \frac{\gamma^{\circ}}{2}$	$u_1(B) = (\gamma^{\circ}/2)x_3$ $u_2(B) = 0$ $u_3(B) = (\gamma^{\circ}/2)x_1$ $\phi(B) = 0$	$U_e = \frac{V}{2} C_{55} (\gamma^{\circ})^2$
C_{66}	$\varepsilon_{12}^{\circ} = \frac{\gamma^{\circ}}{2}$	$u_1(B) = (\gamma^{\circ}/2)x_2$ $u_2(B) = (\gamma^{\circ}/2)x_1$ $u_3(B) = 0$ $\phi(B) = 0$	$U_e = \frac{V}{2} C_{66} (\gamma^{\circ})^2$

Table 5. Boundary conditions for dielectric constants

Property	Applied strain and electric field	Displacements and electric potential	Dielectric energy
κ_1/κ_0	$E_1^{\circ} = E^{\circ}$	$u_1(B) = 0$ $u_2(B) = 0$ $u_3(B) = 0$ $\phi(B) = -E^{\circ}x_1$	$U_d = \frac{V}{2} \kappa_1 (E^{\circ})^2$
κ_2/κ_0	$E_2^{\circ} = E^{\circ}$	$u_1(B) = 0$ $u_2(B) = 0$ $u_3(B) = 0$ $\phi(B) = -E^{\circ}x_2$	$U_d = \frac{V}{2} \kappa_2 (E^{\circ})^2$
κ_3/κ_0	$E_3^{\circ} = E^{\circ}$	$u_1(B) = 0$ $u_2(B) = 0$ $u_3(B) = 0$ $\phi(B) = -E^{\circ}x_3$	$U_d = \frac{V}{2} \kappa_3 (E^{\circ})^2$

Table 6. Boundary conditions for piezoelectric constants

Property	Applied strain and electric field	Displacements and electric potential	Electromechanical energy
e_{15}	$\varepsilon_{13}^{\circ} = \frac{\gamma^{\circ}}{2}$ $E_1^{\circ} = E^{\circ}$	$u_1(B) = (\gamma^{\circ}/2)x_3$ $u_2(B) = 0$ $u_3(B) = (\gamma^{\circ}/2)x_1$ $\phi(B) = -E^{\circ}x_1$	$U_{em} = \frac{V}{2}e_{15}\gamma^{\circ}E^{\circ}$
e_{31}	$\varepsilon_{11}^{\circ} = \varepsilon^{\circ}$ $E_3^{\circ} = E^{\circ}$	$u_1(B) = \varepsilon^{\circ}x_1$ $u_2(B) = 0$ $u_3(B) = 0$ $\phi(B) = -E^{\circ}x_3$	$U_{em} = \frac{V}{2}e_{31}\varepsilon^{\circ}E^{\circ}$
e_{32}	$\varepsilon_{22}^{\circ} = \varepsilon^{\circ}$ $E_3^{\circ} = E^{\circ}$	$u_1(B) = 0$ $u_2(B) = \varepsilon^{\circ}x_2$ $u_3(B) = 0$ $\phi(B) = -E^{\circ}x_3$	$U_{em} = \frac{V}{2}e_{32}\varepsilon^{\circ}E^{\circ}$
e_{33}	$\varepsilon_{33}^{\circ} = \varepsilon^{\circ}$ $E_3^{\circ} = E^{\circ}$	$u_1(B) = 0$ $u_2(B) = 0$ $u_3(B) = \varepsilon^{\circ}x_3$ $\phi(B) = -E^{\circ}x_3$	$U_{em} = \frac{V}{2}e_{33}\varepsilon^{\circ}E^{\circ}$

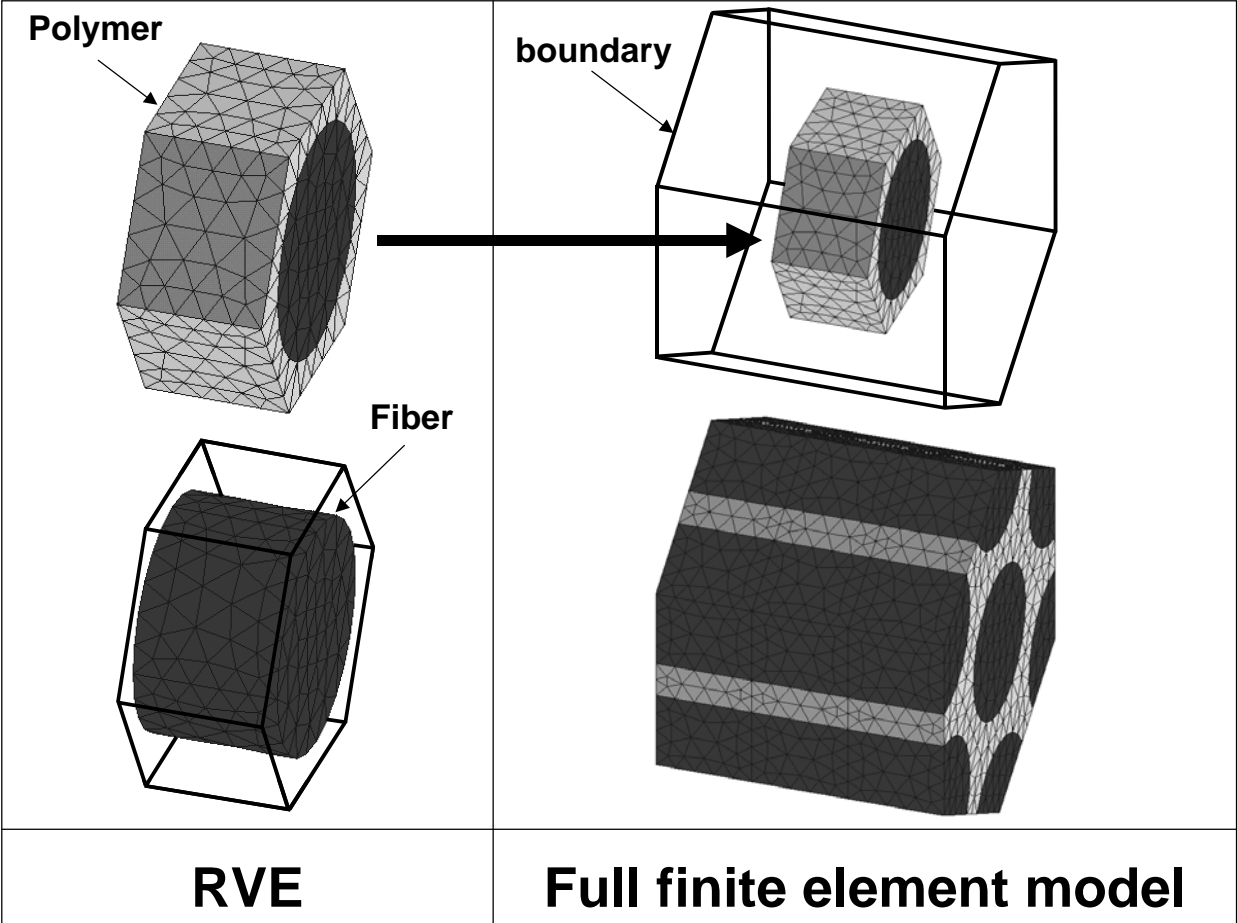


Figure 1. Finite element RVE of fiber composite

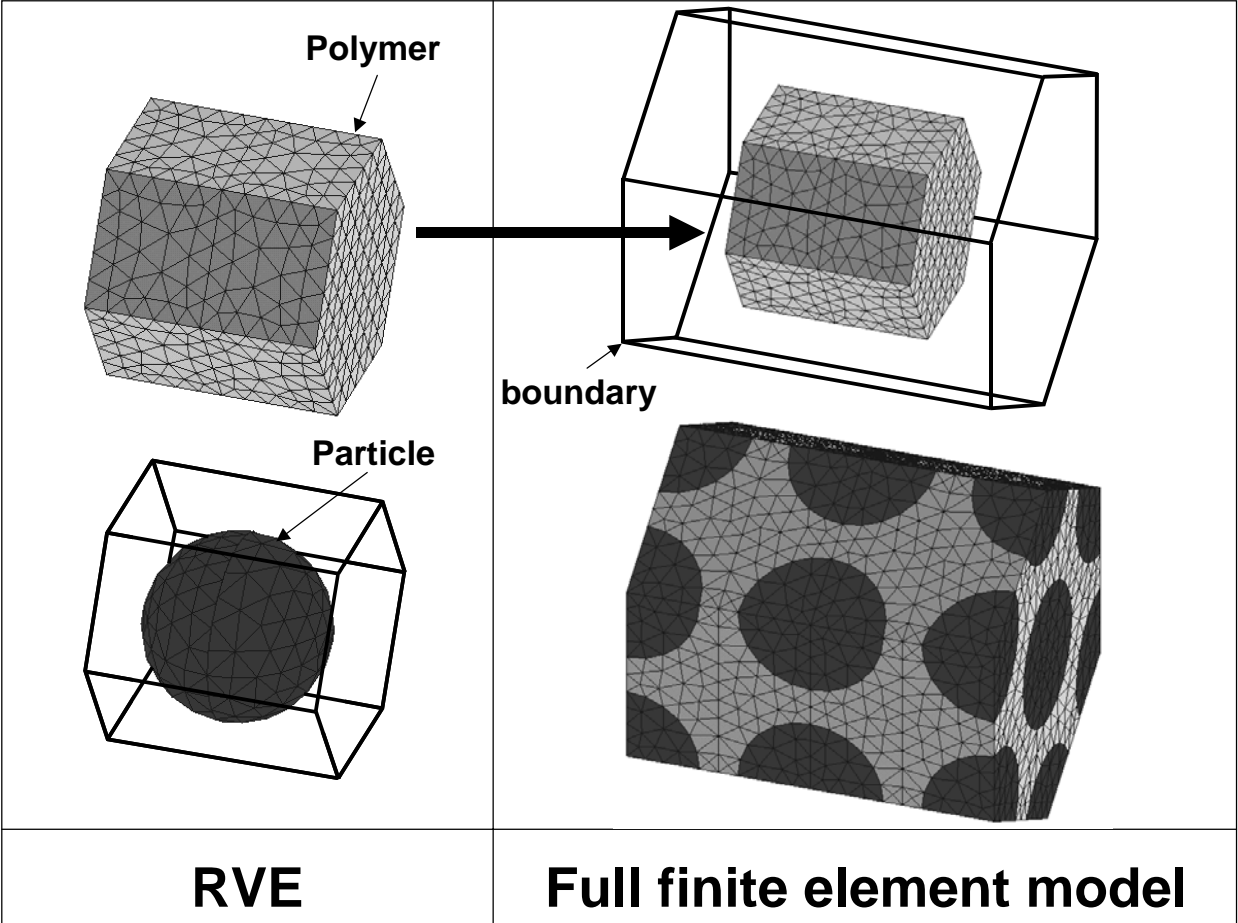


Figure 2. Finite element RVE of particle composite

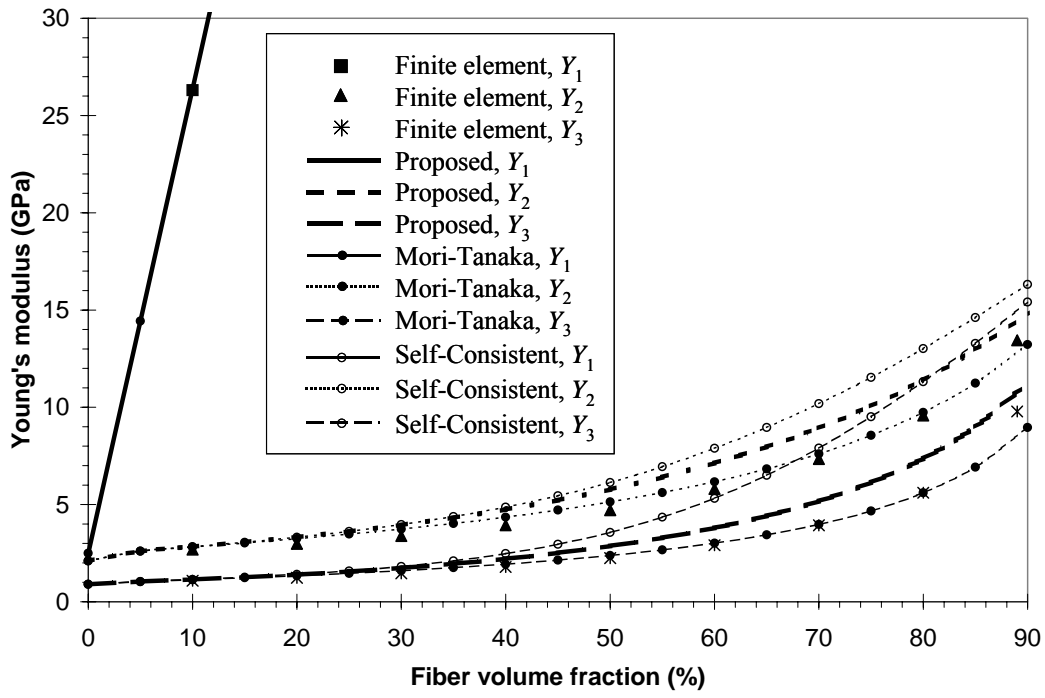


Figure 3. Young's moduli vs. fiber volume fraction for graphite/PVDF composite

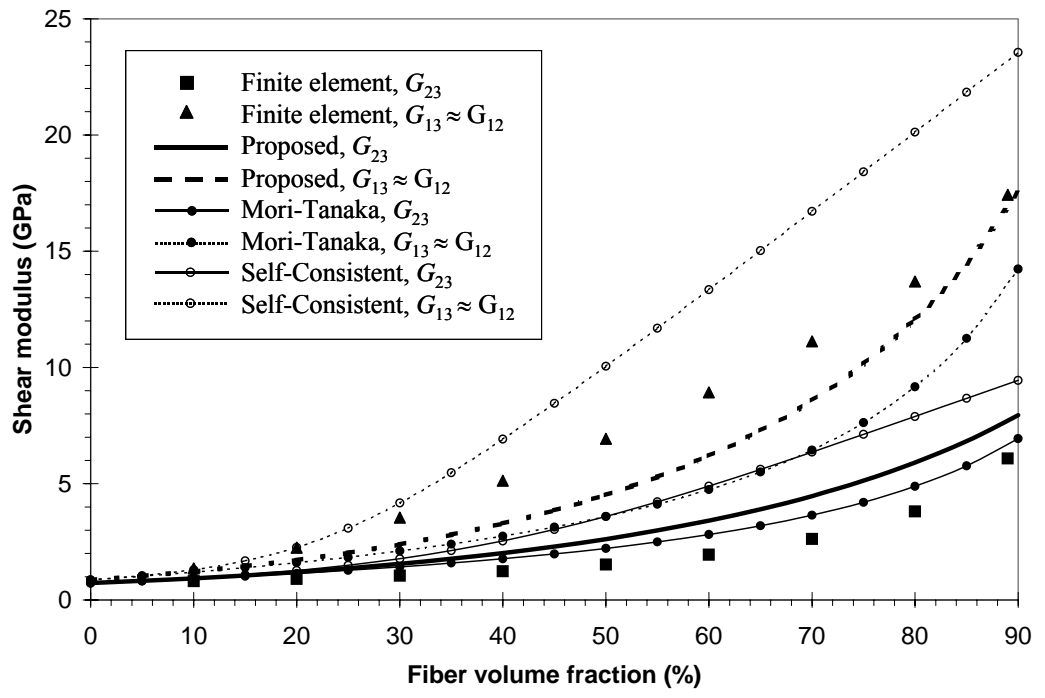


Figure 4. Shear moduli vs. fiber volume fraction for graphite/PVDF composite

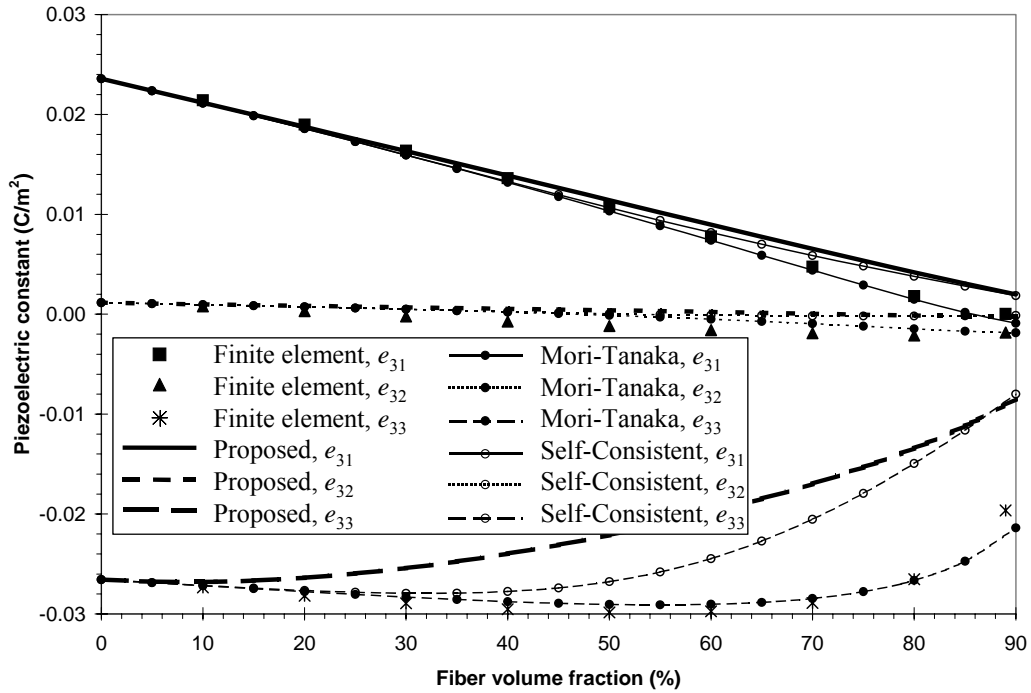


Figure 5. Piezoelectric constants vs. fiber volume fraction for graphite/PVDF composite

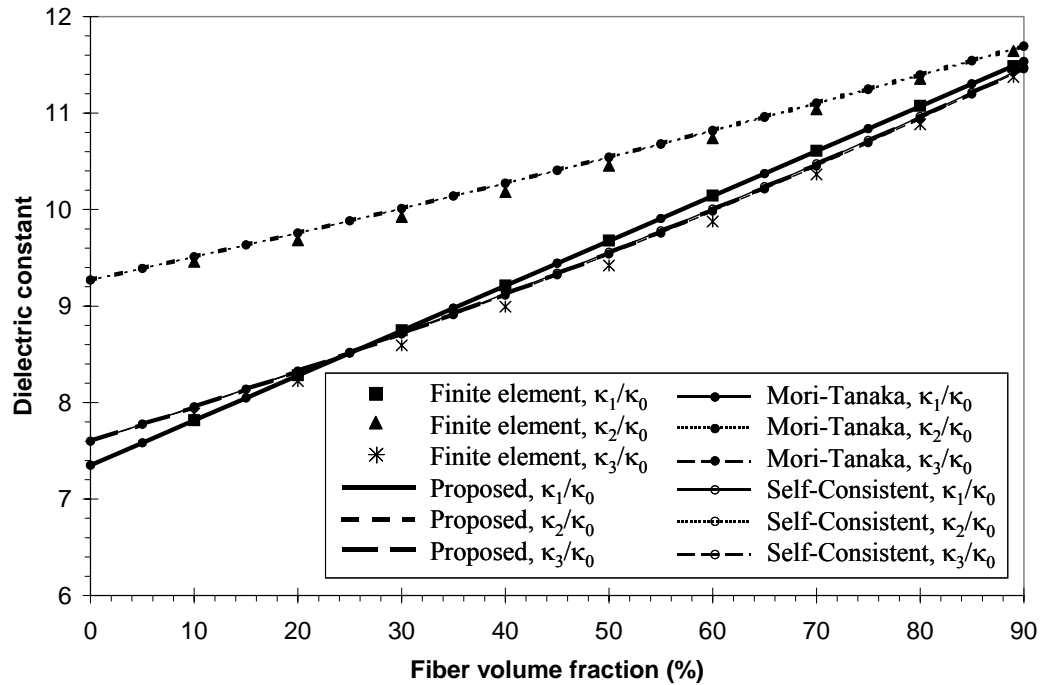


Figure 6. Dielectric constants vs. fiber volume fraction for graphite/PVDF composite

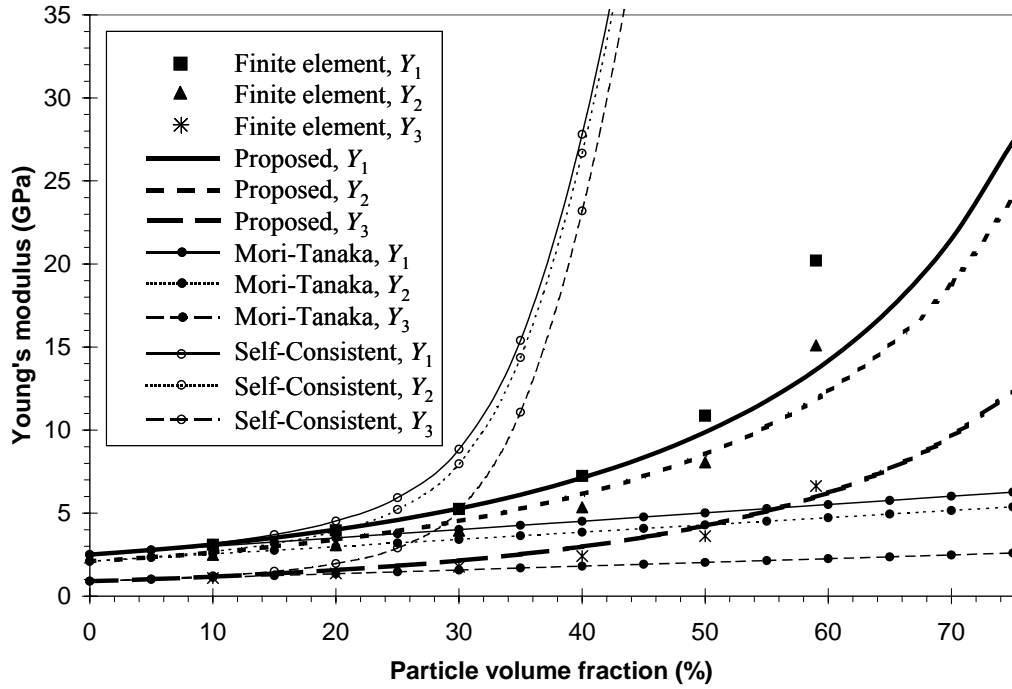


Figure 7. Young's moduli vs. particle volume fraction for SiC/PVDF composite

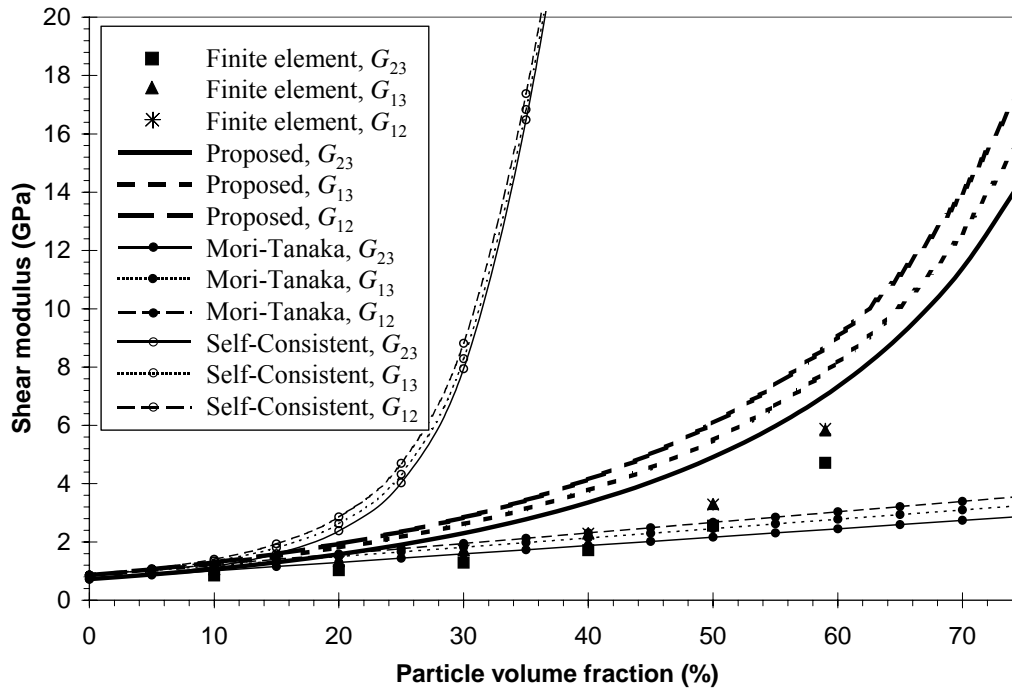


Figure 8. Shear moduli vs. particle volume fraction for SiC/PVDF composite

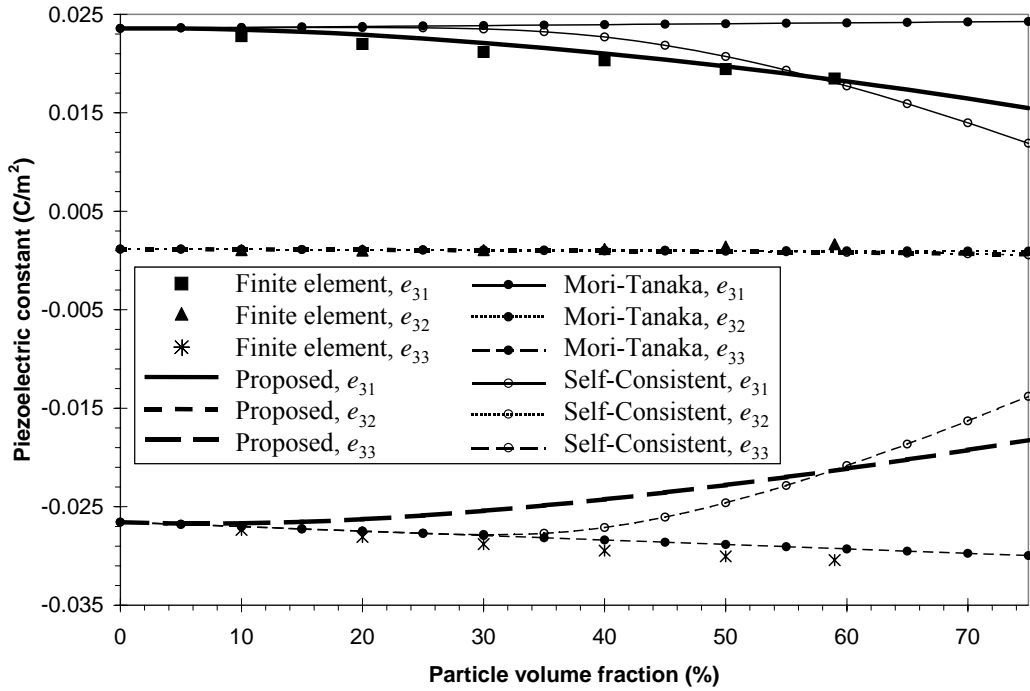


Figure 9. Piezoelectric constants vs. particle volume fraction for SiC/PVDF composite

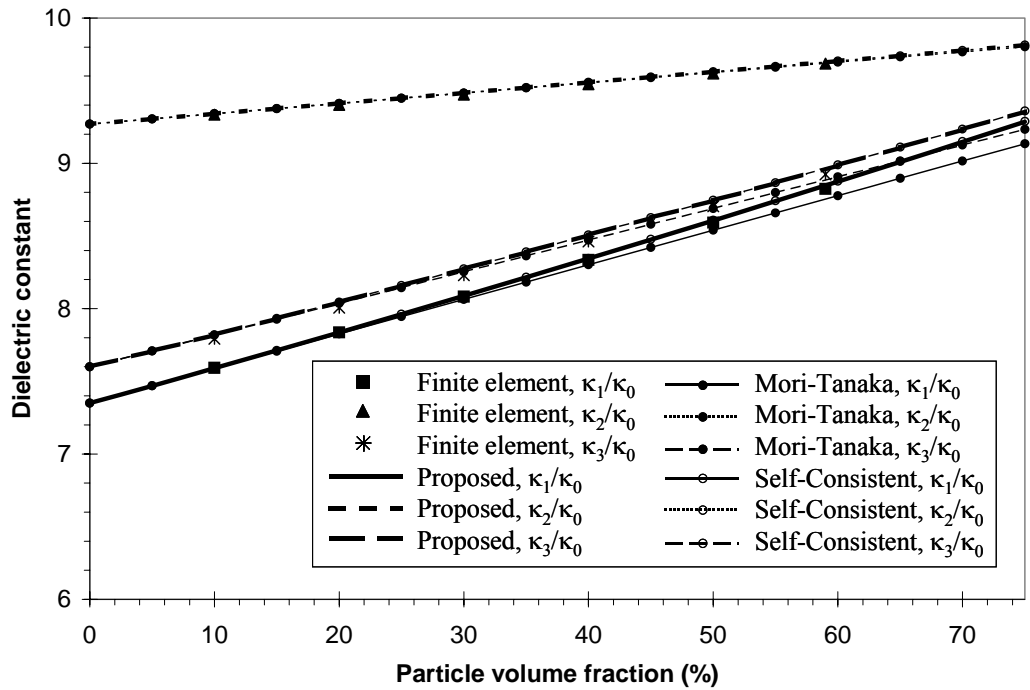


Figure 10. Dielectric constants vs. particle volume fraction for SiC/PVDF composite

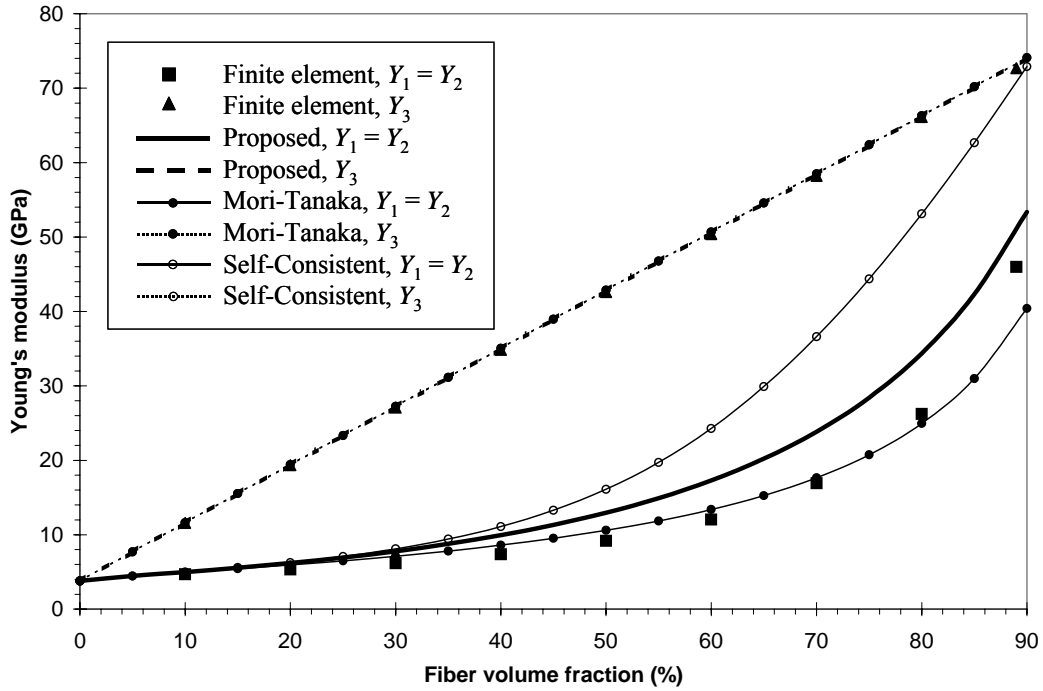


Figure 11. Young's moduli vs. fiber volume fraction for PZT-7A/LaRC-SI composite

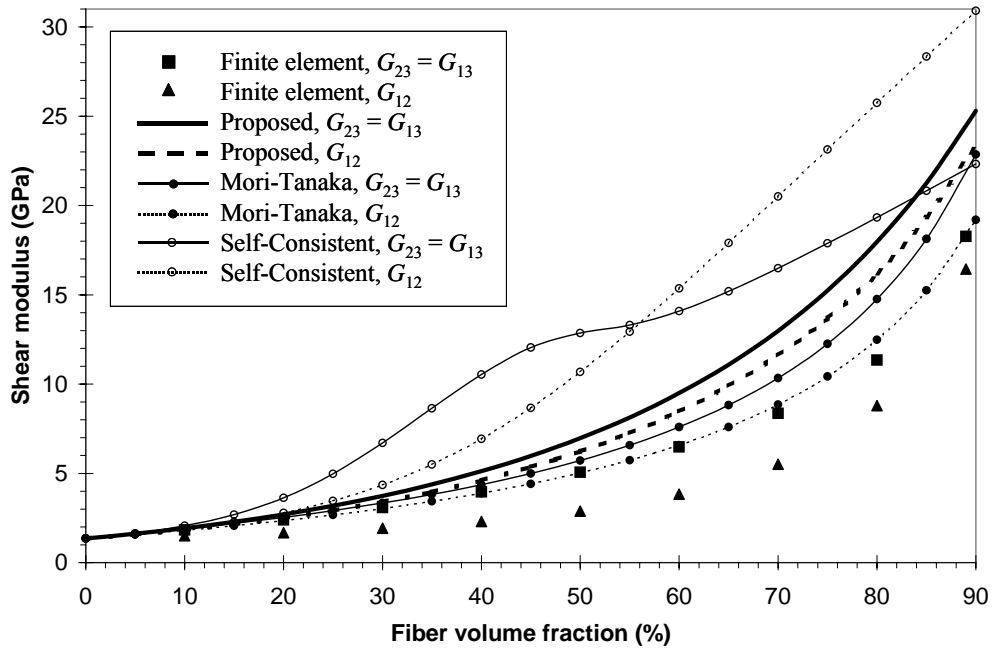


Figure 12. Shear moduli vs. fiber volume fraction for PZT-7A/LaRC-SI composite

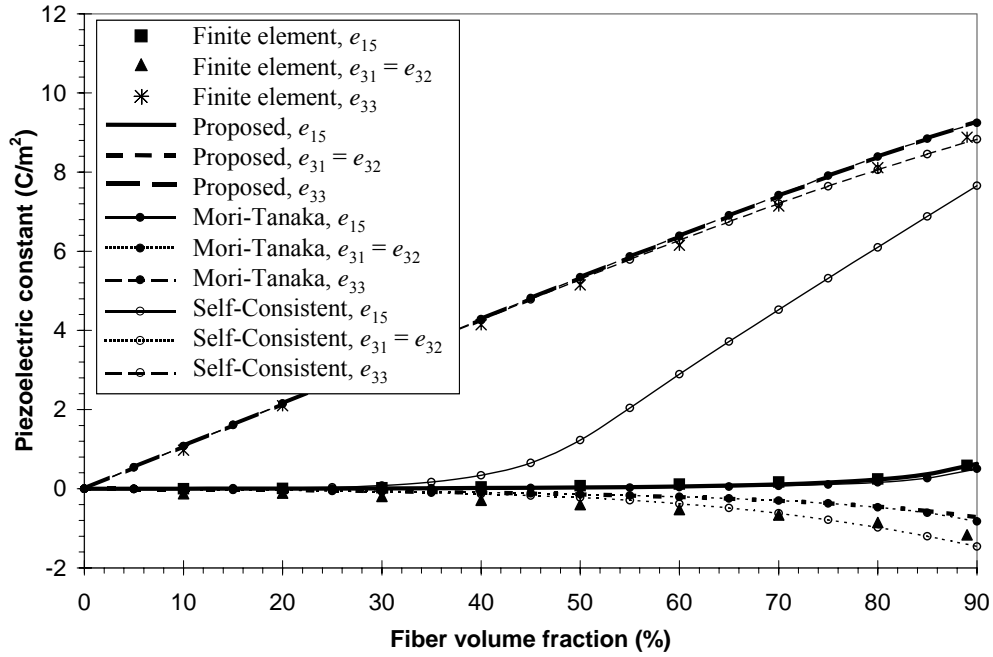


Figure 13. Piezoelectric constants vs. fiber volume fraction for PZT-7A/LaRC-SI composite

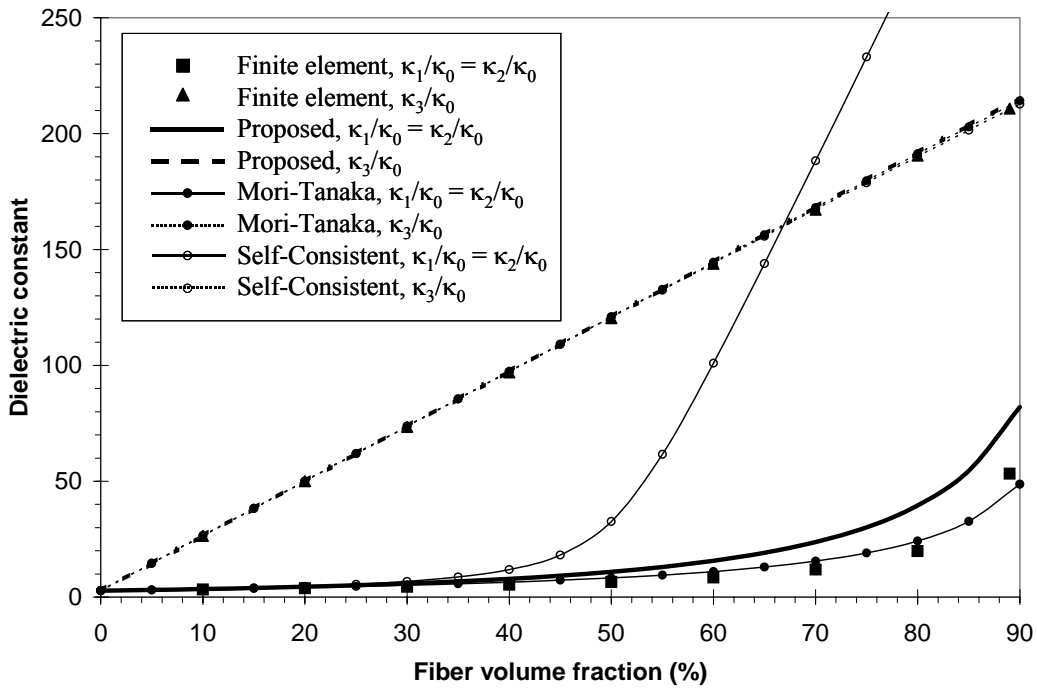


Figure 14. Dielectric constants vs. fiber volume fraction for PZT-7A/LaRC-SI composite

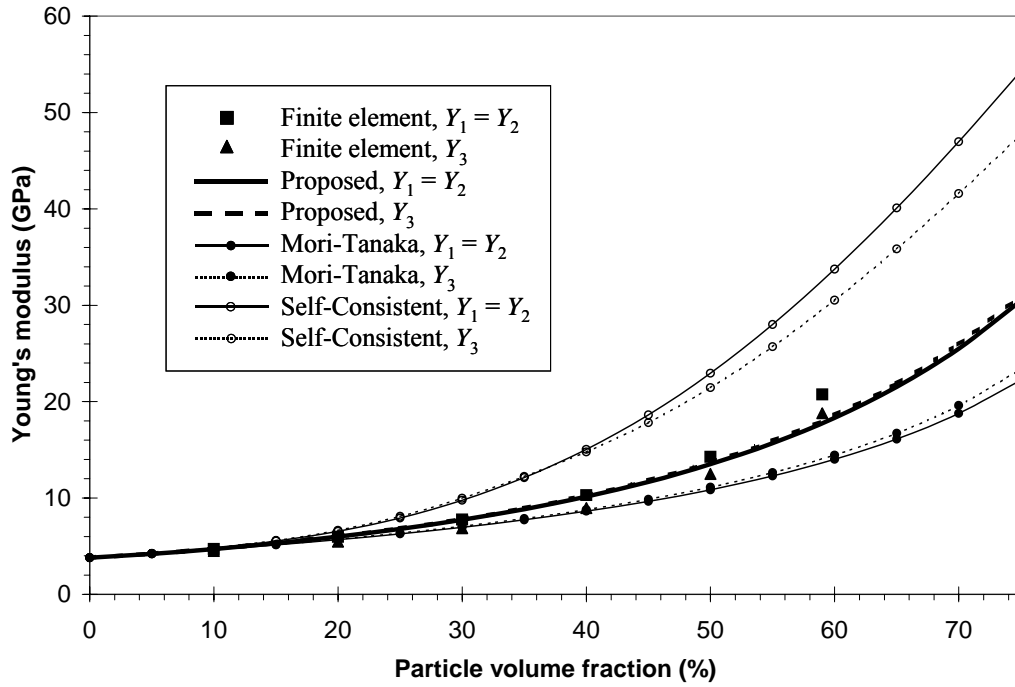


Figure 15. Young's moduli vs. particle volume fraction for PZT-7A/LaRC-SI composite

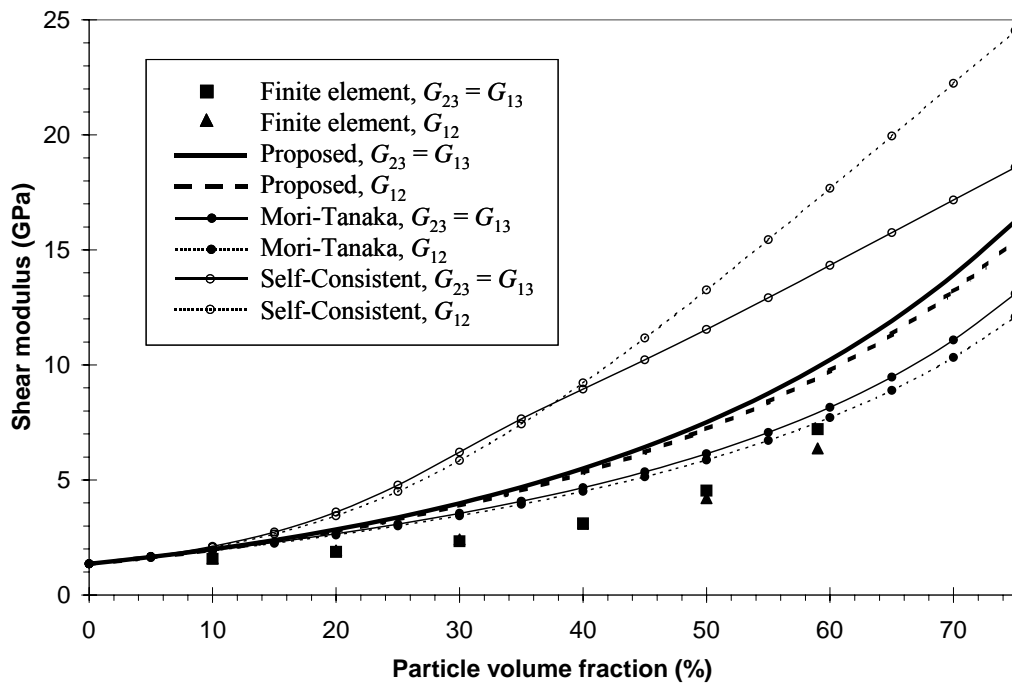


Figure 16. Shear moduli vs. particle volume fraction for PZT-7A/LaRC-SI composite

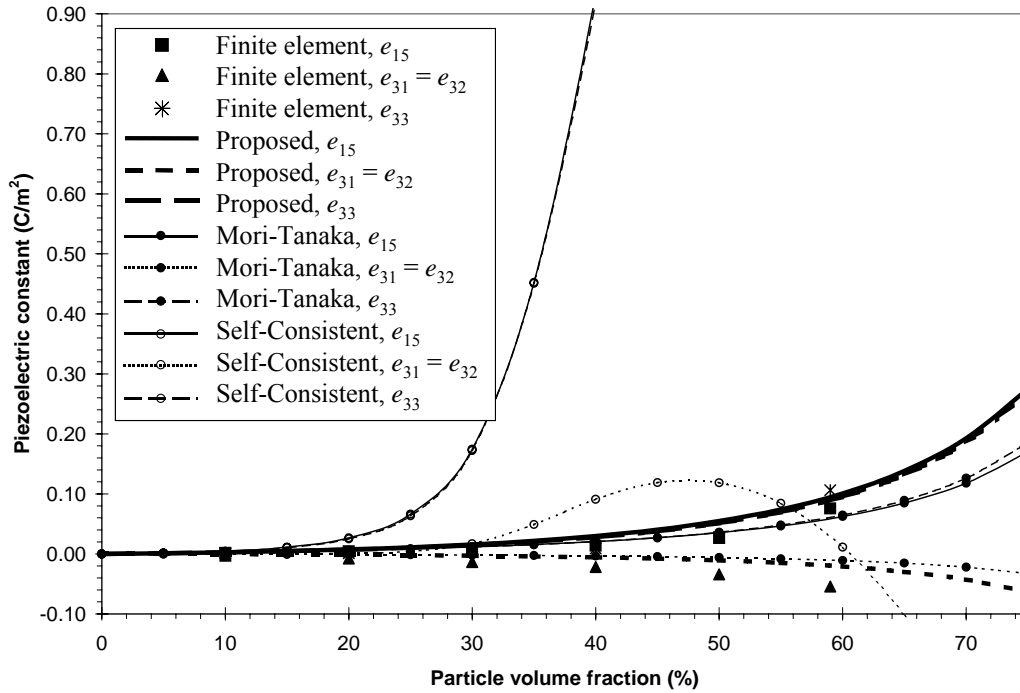


Figure 17. Piezoelectric constants vs. particle volume fraction for PZT-7A/LaRC-SI composite

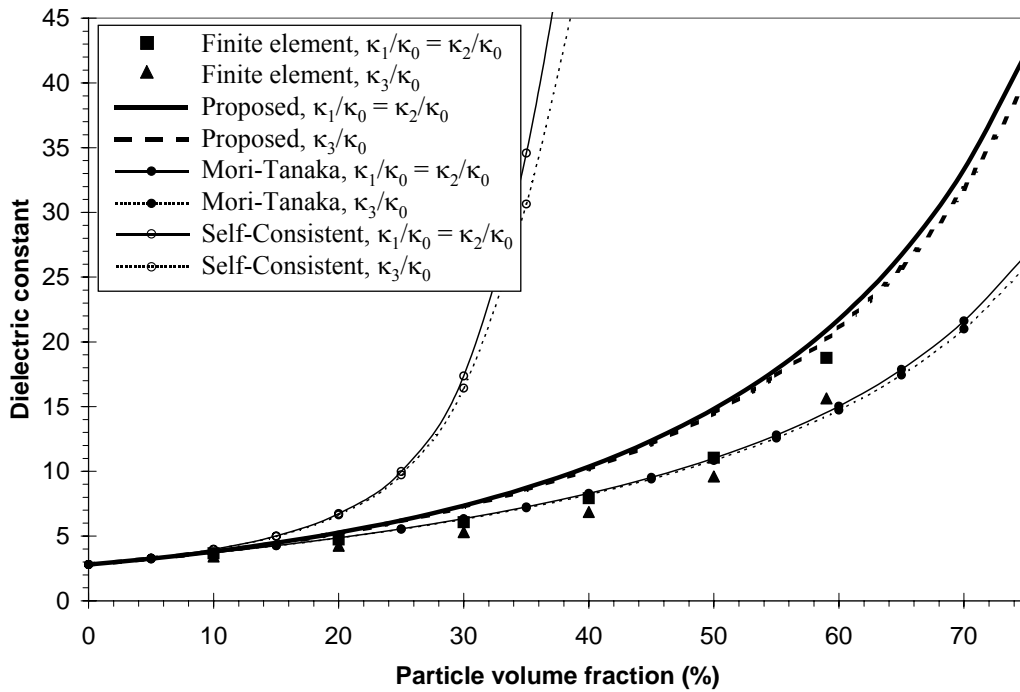


Figure 18. Dielectric constants vs. particle volume fraction for PZT-7A/LaRC-SI composite